



Image Enhancement and Feature Extraction Based on Low-Resolution Satellite Data

M.Dhinakaran¹, P.Vinayagam², K. Madhavipriya³

Assistant Professor, Department of Electronics and Communication Engineering, SKP Engineering College
Tiruvannamalai, Tamilnadu, India^{1,2,3}

ABSTRACT: The purpose of this study is to investigate the sensitivity of contrast-based textural measurements and morphological characteristics that derive from high-resolution satellite imagery (three-band SPOT-5) when diverse image enhancements techniques are piloted. The general framework of the application is the built-up/nonbuilt-up detection. In the existence of a low-resolution reference layer, we apply supervised learning that indirectly reduces the uncertainty and improves the quality of the reference layer. Based on the new class label assignments, the image histogram is adjusted suitably for the computation of contrast-based textural/morphological features. A case study is presented where we test a mixture of image enhancement operations like linear and decorrelation stretching and assess the performance through ROC analysis against available building footprints. Experimental results demonstrate that spectral band combination is the key factor that conditions the contrast of grayscale images. Contrast adjustment (before or after the band combination and merging) supports considerably the extraction of informative features from a low-contrast image; in case of a well-contrasted image, the improvement is marginal.

KEYWORDS: Built-up detection, contrast adjustment, feature extraction, high-resolution image enhancement, low-resolution reference data, morphological, supervised learning, support vector machines (SVMs), textural.

I. INTRODUCTION

In the context of contrast-based feature extraction from high-resolution satellite imagery, image enhancement techniques are utilized to modify the band intensities and decrease the noise that covers significant information. Typical image enhancement techniques are as follows: linear contrast adjustment, decorrelation stretching, histogram equalization, and adaptive filtering [1]–[4] classified as pixel/spatial-based approaches. Fourier decomposition, wavelet transform, and discrete cosine transform [2], [5], [6] are alternative approaches that belong to the frequency-domain techniques. The majority of the aforementioned techniques aim at improving the visual inspection of the image and usually involves manual parameter tuning. The requirements of our application, as delineated further down, impose a fully automated approach combined with a low-complexity algorithm for massive image processing. The framework of the specific application is defined by the following

considerations and assumptions.

- 1) Within the operational project of generating a wall-towall layer of human settlements in Europe, we processed in a massive and automated way more than 2000 very high-resolution (VHR) satellite images provided by the Copernicus European Earth Observation Program by means of the Copernicus Core_003 SPOT5 satellite imagery dataset [7], [8]. These data consist of SPOT-5 images with continental coverage of Europe and the following basic technical characteristics: a) ETRS89 Lambert equal area (LAEA) projection; b) spatial resolution at 2.5 m; and c) three spectral bands: green (bG), red (bR), and near infrared (bNI).
- 2) The images were not calibrated to account for seasonal and atmospheric factors. As such and without further amplification, they have been treated directly by the processing modules.
- 3) The resulting classification was based on textural and morphological features. Analytical description of the features can be found in [10].



International Journal of Advanced Research in Electrical, Electronics and Instrumentation Engineering

(An ISO 3297: 2007 Certified Organization)

Vol. 4, Issue 10, October 2015

The ground for this study shaped from the need of finding a consistent and automatic way for the standardization of the uncalibrated images. Our main goal was to test the sensitivity of contrast-based textural measurements and morphological characteristics when computed over different gray representations. Thereafter, a second objective was the investigation of alternative ways, statistical in their nature, which might provide a suitable means for conducting standardized feature extraction.

Accordingly, we present herein some experimental results and we put forward a statistical learning approach for the stabilization of the image contrast sensitivity to different preprocessing conditions. In particular, a simple algorithmic schema is proposed as described briefly below.

- 1) A binary classifier [support vector machine (SVM)] is trained in the light of a low-resolution reference layer.
- 2) The optimal hyperplane that separates the two classes: 1) built-up (BU); and 2) nonbuilt-up (NBU) is estimated through a nonlinear mapping.
- 3) The class labels of the reference layer are modified via *ad hoc* treatment of the respective training samples that delimit the hyperplane into a high-dimensional feature space.
- 4) A histogram adjustment driven by the reference layer is applied per class. In practice, this turns out to instruct and facilitate mostly the extraction of the textural measurements.

For the needs of supervised learning, we exploited the existence of the soil sealing layer (SSL). This is a raster dataset of European areas providing information of the degree of soil sealing in aggregated spatial resolution of 100 m \times 100 m [11]. Main traits of the specific product are its completeness and its relatively high overall accuracy, observed largely in dense BU areas [12].

The proposed approach constitutes a data preparation phase just before the feature extraction. It attempts to improve the quality of the textural/morphological characteristics while retaining the computational burden in low levels. Generally speaking, it moves inside the concept of synergy between machine learning and image processing; one contiguous application has been presented recently in [13].

This paper is organized as follows. Section II describes the algorithmic schema, the assumptions, and the parameterization. Section III explains the experimental setup; results are demonstrated for the city of Torino, Italy, while the performance is assessed through *ROC* analysis with the aid of a footprint layer at 2.5-m spatial resolution. Section IV discusses the findings of the experimental study and Section V summarizes and provides suggestions for future work.

II. SCHEMA DEFINITION

A. IMAGE FEATURES

The textural measurements we are interested in are estimated through the Haralick's measure for the intensity contrast between a pixel and its neighbors [14]. The factors (quantization, length, and orientation) and the operators like fuzzy composition are defined in [15]; the produced textural layer is known as PANTEX.

Regarding the morphological features, we included in our tests a recently introduced index named *morphological building index* (MBI) [16], [17]. It is a quite accurate indicator that considers the characteristics of buildings (brightness, size, contrast, directionality, and shape) by integrating multiscale and multidirectional morphological operators. Note that both PANTEX and MBI are automatic indices and their operation is not based on statistical learning and training samples.

Trying to reduce the high dimensionality of the cooccurrence matrix over which the textural measurements are computed, we convert the multiband images to 8-bit grayscale. Besides, the graylevel images are suitable to work with

International Journal of Advanced Research in Electrical, Electronics and Instrumentation Engineering

(An ISO 3297: 2007 Certified Organization)

Vol. 4, Issue 10, October 2015

morphological operators. The challenge now is to adjust selectively the image intensities, so that the difference between the pixel values that refer to BU and NBU to be as high as possible; in this manner, the BU representation becomes distinguishable. The contrast adjustment can be done either during the image conversion to grayscale by means of a suitable spectral band combination or by modifying the histogram of the image intensities.

B. SYLLOGISM

The typical reasoning of supervised learning suggests the use of a BU/NBU template to drive the contrast tuning. Given that the specific application has to do with satellite images that cover European regions, we employ the SSL as BU/NBU reference. Since the meaning of the SSL range of values does not correspond confidently to an absolute BU/NBU template, some experimentation (several thresholds were tested over 60 scenes and their effectiveness was validated through visual inspection) guided us to apply two thresholds $SSL \geq 50 \wedge SSL \leq 100$ to make the layer binary, with ones indicating all the medium-to-high probability BU areas. Nevertheless, the disparity in terms of spatial resolution (a ratio of 40) between SSL and the SPOT-5 images used for processing makes their direct association problematic. Fig. 2(a) and (b) clearly shows the distance between SSL and the reality represented by the building footprints (BFs). The coarse resolution of SSL inserts uncertainty and hinders the distinction of BU pixels in the high-resolution imagery.

Apart from directly using the upsampled SSL as reference layer, we elaborated the process of downscaling the layer in a statistical fashion. The simple idea we introduce in this paper is to seek for the hyperplane that separates tuples of spectral values, derived from the input images, into two groups (BU/NBU) according to the reference layer in its original (low) resolution. For this purpose, we employ a powerful classification technique like the SVM which draws the optimal hyperplane that linearly discriminates the two classes BU/NBU into a high-dimensional feature space H without using an explicit mapping. This can be achieved by means of the *kernel trick* [18], [19]. *Support vectors* (SVs) are the closest tuples of measurements to the hyperplane with respect to H ; consequently, they contain the critical information for the class separation. In our application, having as fact that the reference layer does not constitute an accurate template mainly due to its low spatial resolution, the meaning of SVs matches with the concept of uncertainty that is inherent along the class boundaries. Thereafter, three options are deemed for the SVs usage.

- 1) To totally remove their respective class labels from the reference layer: this decision targets at the increase in both intra-class similarity and inter-class dissimilarity; however, it has high risk due to the loss of potentially useful information for the discrimination of the classes.

the SVs and b is the bias.

Then, we generate a new reference layer by following one of the three options described in Section II-B.

$$\begin{cases} y_j, & j \in V \\ 0, & \text{otherwise} \end{cases}$$

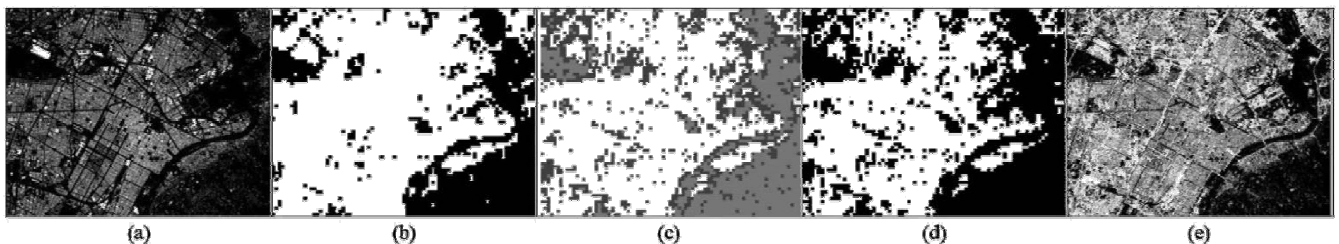


Fig. 1. Two experimental configurations.

International Journal of Advanced Research in Electrical, Electronics and Instrumentation Engineering

(An ISO 3297: 2007 Certified Organization)

Vol. 4, Issue 10, October 2015

1) $SSL(2)k =$

$$2) SSL_k^{(3)} = \begin{cases} y_j, & j \in V \\ -1, & \text{otherwise} \end{cases}$$

3) Build a new SVM by using $X = [x_j] \forall j \in V$ as training set and define the respective discrimination function. Subsequently, utilize this function to classify the pixels of the original image $Imm \times 3$. The resulting binary image

(4)

sents SSL_m the $\times n$ becomes downscaled the version new reference. of SSL Actually, (1). Note it that pre-the

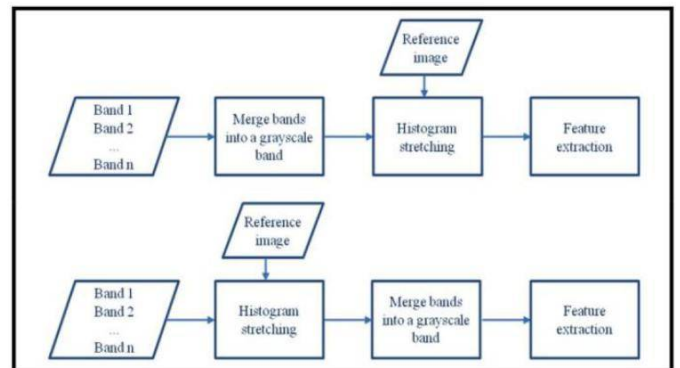
number of SVs derived from the second SVM is 30 – 40 times less than the number of the first SVs. This reduces

$$\max \sum a_i - \frac{1}{2} \sum \sum a_i a_j y_i y_j K(x_i, x_j)$$

$$\sum a_i y_i$$

$$K(x_i, x_j) = \langle \Phi(x_i), \Phi(x_j) \rangle$$

$$f(x) = \sum_v a_v y_v K(x, x_v) + b$$



D. CONTRAST ADJUSTMENT

The last processing stage refers to the adjustment of the image histogram. At this point, we explore two scenarios. (C1) The original image is converted to grayscale, and then, the contrast adjustment takes place. (C2) The histogram adjustment is done separately for each band of the original image (multichannel histogram stretching), and then, the bands are merged to form a grayscale image. Fig. 1 displays the two experimental scenarios using flow charts. In both cases, the operation occurs in the spatial domain of size $m \times n$. Accordingly, $SSL_k^{(1)}$, $SSL_k^{(2)}$, $SSL_k^{(3)}$ become

$$SSL_{m \times n}^{(1)}, SSL_{m \times n}^{(2)}, SSL_{m \times n}^{(3)} \text{ through nearest neighbor (NN)}$$

interpolation. All the reference images are displayed in Fig. 2.

Let $Bm \times n$ denote the input image and $SSL_m \times n$ represent one of the four available reference images. Herein, we describe and



International Journal of Advanced Research in Electrical, Electronics and Instrumentation Engineering

(An ISO 3297: 2007 Certified Organization)

Vol. 4, Issue 10, October 2015

Fig. 2. Reference layers at 2.5-m spatial resolution: (a) City of Torino: building footprints covered an area of 6.5×8.24 km; (b) $SSL^{(1)}$; (c) $SSL^{(2)}$; (d) $SSL^{(3)}$; and (e) $SSL^{(4)}$. The images in (b), (c), and (d) have been resized via *nearest neighbor* interpolation to match the resolution of the input image. In put in the test eight different computations for the stretching of image values

$$\forall l : y_l = -1 \vee y_l = 1, \quad y_l \in SSL_{m \times n}$$

$$\rightarrow p_l^{updated} = \frac{\min(\max(p_l, a), b) - a}{b - a}, \quad p_l \in B_{m \times n}$$

(M1.1) Where $a = \bar{p}_l - r s_{p_l}$ and $b = \bar{p}_l + r s_{p_l}$ with p^{-l}

denoting the mean of p_l and s_{p_l} denoting the respective standard deviation; $r = 2$ for both classes.

(c), the darker pixels have been omitted completely.

(M1.2) The same as in (M1.1), $r = \begin{cases} 1, & y_l = 1 \text{ but} \\ 2, & y_l = -1 \end{cases}$

(M1.3) The same as in (M1.1), $r = \begin{cases} 2, & y_l = 1 \\ 1, & y_l = -1 \end{cases}$ but

(M1.4) The same as in (M1.1) but for the class 1, i.e., only the values that refer to BU are modified, whereas the other values remain intact.

(M2.1) $a = \max(\min(p_l, r1)$ and $b = \min(\max(p_l, r2)$, $r1 = 0$, $r2 = 255$

(M2.2) The same as in (M2.1) but $r1 = 0.1 * 255$ and $r2 =$

$0.9 * 255$.

(M2.3) The same as in (M2.1) but only for the class 1. (M2.4) The same as in (M2.2) but only for the class 1.

III. EXPERIMENTAL SETUP

The central question in this paper is whether a low-resolution reference layer can improve the contrast adjustment of an image. A further significant issue in the case of a positive answer is to find the most effective processing stage: during image conversion to grayscale via a good band combination or through operations over the image intensities?

In order to test the band combinations, we established seven scenarios. (O1) $RG_{max} = \max(bR, bG)$ refers to the maximum decomposition of a multichannel image and results in a brighter grayscale image. It is also related to the *Value* component of the HSV color model. (O2) $RG_{linear} = 0.3559bR + 0.6441bG$ constitutes a modification of *luma* that is defined as the weighted average of gamma-corrected *RGB*; it is a standard band combination fitted on how human eye perceives



International Journal of Advanced Research in Electrical, Electronics and Instrumentation Engineering

(An ISO 3297: 2007 Certified Organization)

Vol. 4, Issue 10, October 2015

color. The weight for the blue band has been shared equally to the other two weights. (O3) $RGNlinear = 0.2989bR + 0.5870bG + 0.1140bNI$: the *luma* linear combination with the blue band to have been substituted by the infrared. (O4)

$NIRGlinear = 0.2989bNI + 0.5870bR + 0.1140bG$: the same weights as in (O3) but following a different band order; the

next linear combinations (O5) $RGlinearD$, (O6) $RGNlinearD$, and (O7) $NIRGlinearD$ are defined in the same way as (O2), (O3), and (O4), respectively, with the difference that the bands are the decorrelated versions of the original ones. The specific application of decorrelation stretch keeps the same image statistics in both input and output images. At the end, we tested 7 input images \times 2 histogram adjustment scenarios \times (4 reference layers + 1 test without reference) \times 8 ways of contrast stretching = 560 cases.

Regarding the SVM parameter settings, the *Gaussian radial basis function* (RBF) was selected as kernel

$$K(x_i, x_j) = \exp\left(-\|x_i - x_j\|^2 / 2\sigma^2\right)$$

with $\sigma = 0.6$ width/scaling factor; the control parameter C was set to 1 for all the vectors. The hyper-parameters were defined and optimized through cross-validation, using as test cases areas where BFs are available. As regards the kernel selection, we also experimented with the linear and the quadratic kernel, mainly due to their relatively low computational cost; however, the Gaussian *RBF* kernel turned out to define better the separation hyperplane and to capture the nonlinearity in the original feature space. Concerning the extraction of the textural measurements, a squared window of size 25 m was considered suitable for the computation of cooccurrence matrices at 2.5-m resolution. For the MBI, we selected four directions (45° , 90° , 135° , and 180°) and three scales (5, 17, and 29).

The case study we demonstrate here has been elaborated over the city of Torino, Italy, where BFs are available. The assessment of the results was done with the aid of *ROC* analysis by computing the *area under curve* (AUC) and the *equal error rate* (EER) [10] between PANTEX/MBI and BFs; Tables I–IV display those results. Table V shows the degree of agreement between BFs and each of the reference layers at 2.5 m. Two performance measures that are deemed more appropriate in case of imbalanced datasets are reported in this table: balanced accuracy (average of sensitivity and specificity) and F-score (harmonic mean of precision and recall/sensitivity). Fig. 3 shows some indicative snapshots of the three-band input images, their grayscale composition, and their respective binary version of PANTEX after applying the EER threshold. The pictures in Fig. 4 demonstrate the matching degree between MBI and BFs in two built-up cases: dense and sparse. In all the aforementioned cases, we do not make use of the NDVI, which surely improves the BU detection.

Finally, Fig. 5 shows how the histogram of the original threeband image is amended through different types of grayscale conversion and contrast stretching. Picking out the maximum value of an RGB triplet is the most common approach for

preparing the input image to the PANTEX and MBI algorithms; when applied to the specific SPOT-5 images, the *RGmax* conversion produces a grayscale histogram that is very similar to the one given by the green band itself [Fig. 5(a) and (b)]. Moreover, the majority of the image values are located in a specific brightness range, resulting in a moderate contrast. Fig. 5(c) shows how decorrelation stretching normalizes and distributes a

little better the values over the dynamic range; however, it gathers the majority of the values around the mean value. Fig. 5(d) demonstrates a reference-based contrast stretching that seems to spread the image values throughout the range quite evenly. Based again on the reference, it impels the distinction of the gray levels by introducing artificially a bimodal behavior over the image data.

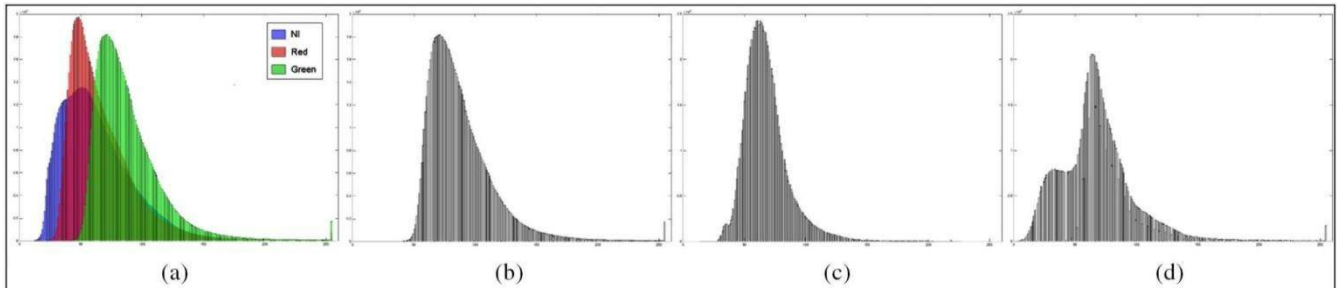


Fig. 5. Image histogram and contrast stretching: (a) three-band histogram of the original image; (b) RG_{max} ; (c) $NIRG_{linearD}$; (d) $RG_{max} \rightarrow$

detected corners. The probability of a pixel to represent a corner increases proportionally to the distinction level between this pixel and its neighborhood. That is, a contrast adjustment that sharpens enough the grayscale image has the potentiality to boost the derivation of prominent textural characteristics. The morphological features instead, and especially those that derive from multiscale analysis, turn out to be more stable against the contrast

(M2.1)| $SSL^{(4)}$ | (C1).

variations. The successive use of structural elements of increasing size and the subsequent process of differentiating between objects detected at dissimilar scales somehow manage to compensate the influence of a moderate contrast. Besides, the morphological characterization has to do, not only with brightness and contrast but also takes into consideration the size and the shape of the objects to be detected.

2) The feature extraction as described herein requires a grayscale image as input. The typical approach for the calculation of both PANTEX and MBI is to provide as input an image consisting of the maximum values of the RGB triplet. However, the experimental results show that there are other band combinations (like the $luma$, with or without decorrelation stretching) that, in many cases, lead to a better contrast. Selecting the right band combination seems to be a key factor especially for the extraction of good textural measurements.

3) The results show that in some cases (M1.4, M2.4, M1.2), the reference-based contrast adjustment can boost the performance. As we explained previously, PANTEX is strongly dependent from the contrast

level; the use of a detailed reference layer (like $SSL^{(4)}$), which makes feasible the contrast correction in smaller image areas, appears to fit better with the second-order statistics and the single-scale processing that the PANTEX algorithm utilizes. On the contrary, MBI appears to work better with a moderate contrast level and starts to show instability at higher levels of image sharpness. Good contrast stretching approaches for MBI can consider the cases (M1.2) and (M1.4).

4) In the two scenarios (C1) and (C2), the stage at which the histogram adjustment takes place is examined. No significant difference or notable effect in terms of performance is observed from the results [exceptions are the

PANTEX cases (M1.4) and (M2.4) using learning against $SSL^{(4)}$]. Hence, we conclude that the histogram

adjustment before or after the image conversion to grayscale leads, in average, to similar outcome.



International Journal of Advanced Research in Electrical, Electronics and Instrumentation Engineering

(An ISO 3297: 2007 Certified Organization)

Vol. 4, Issue 10, October 2015

V. CONCLUSION

Image enhancement and contrast adjustment play a substantial role for the extraction of trustworthy textural and morphological characteristics. In order to investigate and measure the sensitivity of those features against variations in contrast, a series of tests were carried out; different scenarios were examined regarding mainly the image bands' combination and the image histogram adjustment guided by low-resolution reference data. From the reported results, a number of approaches can be distinguished for improving the image contrast and for instructing effectively the feature extraction.

Finally, a meaningful result of this work is the introduction of a simple and relatively fast approach that can "correct" the low-resolution reference and transfer it smoothly in finer resolutions (the $SSL^{(4)}$ case).

Future work includes tests with adaptive histogram adjustment, usage of different reference layers, and application of radiometric feature selection and transformation techniques. The presented work is in experimental phase and still remains to be scaled up and adapt to the conditions of the operational mode.

REFERENCES

- [1] F. Y. Shih, *Image Processing and Pattern Recognition-Fundamentals and Techniques*. Hoboken, NJ, USA: Wiley, 2010.
- [2] R. C. Gonzalez and R. E. Woods, *Digital Image Processing*, 2nd ed. Englewood Cliffs, NJ, USA: Prentice Hall, 2002.
- [3] S. Kim, W. Kang, E. Lee, and J. Paik, "Wavelet-domain color image enhancement using filtered directional bases and frequency-adaptive shrinkage," *IEEE Trans. Consum. Electron.*, vol. 56, no. 2, pp. 1063 – 1070, May 2010.
- [4] A. R. Gillespie, A. B. Kahle, and R. E. Walker, "Color enhancement of highly correlated images. I. Decorrelation and HSI contrast stretches," *Remote Sens. Environ.*, vol. 20, no. 3, pp. 209–235, Dec. 1986.
- [5] H. Demirel, C. Ozcinar, and G. Anbarjafari, "Satellite image contrast enhancement using discrete wavelet transform and singular value decomposition," *IEEE Geosci. Remote Sens. Lett.*, vol. 7, no. 2, pp. 333–337, Apr. 2010.
- [6] G. Srilekha, V. K. Kumar, and B. Jyothi, "Satellite image resolution enhancement using DWT and contrast enhancement using SVD," *Int. J. Eng. Res. Technol. (IJERT)*, vol. 2, no. 5, pp. 1227–1230, May 2013.
- [7] [Online]. Available: <http://cidportal.jrc.ec.europa.eu/copernicus/services/webviewer/core003>
- [8] S. Ferri *et al.*, "A new map of the European settlements by automatic classification of 2.5m resolution SPOT data," in *Proc. IEEE Int. Geosci. Remote Sens. Symp. (IGARSS)*, Quebec City, QC, Canada, Jul. 2014, pp. 1160–1163.
- [9] A. Burger, G. Di Matteo, and P. J. Åstrand, "Specifications of view services for GMES Core_003 VHR2 coverage," European Commission, JRC Tech. Rep., 2012, doi: 10.2788/21898.
- [10] M. Pesaresi *et al.*, "A global human settlement layer from optical HR/VHR RS data: Concept and first results," *IEEE J. Sel. Topics Appl. Earth Observ. Remote Sens.*, vol. 6, no. 5, pp. 2102–2131, Oct. 2013.
- [11] [Online]. Available: <http://www.eea.europa.eu/articles/urban-soilsealing-in-europe>
- [12] G. Maucha, G. Büttner, and B. Kosztra, "European validation of GMES FTS soil sealing enhancement data," European Environment Agency, Final draft, Jun. 2010.
- [13] G. K. Ouzounis, V. Syrriis, and M. Pesaresi, "Multiscale quality assessment of global human settlement layer scenes against reference data using statistical learning," *Pattern Recognit. Lett.*, vol. 34, no. 14, pp. 1636– 1647, Oct. 2013.
- [14] R. M. Haralick, K. Shanmugan, and I. Dinstein, "Textural features for image classification," *IEEE Trans. Syst. Man Cybern.*, vol. 3, no. 6, pp. 610–621, Nov. 1973.
- [15] M. Pesaresi, A. Gerhardinger, and F. Kayitakire, "A robust built-up area presence index by anisotropic rotation-invariant textural measure," *IEEE J. Sel. Topics Appl. Earth Observ. Remote Sens.*, vol. 1, no. 3, pp. 180 – 192, Sep. 2008.